Chapter 4

Viscosity-Enhanced Mechanism for Biogenic Ocean Mixing

4.1 Introduction

Ocean fluid dynamics are unique because of the vertical stratification (of salts and temperature) that inhibits mixing across surfaces of constant density or isopycnals [79, 3, 44, 62, 77]. Additional work is required to transport nutrients and other fluid properties (i.e., dissolved oxygen and heat) against the stratification in the ocean [128]. In order for these properties to be replenished in the whole ocean, mixing of fluid across isopycnals (or diapycnal mixing) is necessary. To estimate the rate of deep ocean mixing, Munk [88] balanced the contributions to heat transfer between advective and diffusive processes. From these calculations, the average vertical eddy diffusion coefficient of heat at abyssal depths was found to be greater than the molecular thermal diffusivity coefficient, implying that molecular diffusion alone cannot transfer heat fast enough in the abyssal ocean [88]. Therefore, other physical mixing processes (i.e., double-diffusive convection, tidal mixing over rough topography, surface winds, and breaking internal waves in midwater) have been identified as energetic inputs to maintain fluid transport in the ocean [63, 87, 117]. However, based on estimates of the energy budget required to maintain deep ocean mixing [89], our knowledge of mixing sources in the ocean is incomplete [142]. Recent scientific efforts suggest that biologically induced mixing may close the energy budget [35, 74, 67].

Observations of biologically generated turbulence in the ocean have led to conflicting conclusions

regarding the significance of the contribution of animal swimming to ocean mixing. Measurements indicate elevated turbulent dissipation in the vicinity of large populations of planktonic animals swimming in concert [74]. From analysis of the microstructure shear spectra, the enhancement of turbulent dissipation by schooling euphasiids are comparable with levels caused by winds and tides [74]. However, it has also been noted that elevated turbulent dissipation is by itself insufficient proof of substantial biogenic mixing [135]. Smaller plankton, which are more numerous in the ocean, inject turbulent kinetic energy at length scales proportional to the animal size. Since much of the turbulent kinetic energy of small animals is injected below the Ozmidov buoyancy length scale, it is primarily dissipated as heat by the fluid viscosity before it can affect ocean mixing at larger length scales [127, 135]. Therefore, the effectiveness of animal swimming on mixing the fluid column, or mixing efficiency [79, 44, 94], is expected to be very low for smaller, more numerous marine animals [135]. Ongoing debate regarding biogenic mixing has focused on comparisons between animal wake turbulence and ocean turbulence [59, 35], however these results are inconclusive in terms of mixing in the ocean [135].

Here we show that a second, previously neglected mechanism of fluid transport by swimming animals is the dominant mechanism of biogenic mixing. Sir Charles Galton Darwin, the grandson of the *Origin of Species* author, first described a mechanism of fluid mixing by a solid object that does not require the object to generate rotational or shearing motion in the flow [34]. As the solid body travels through fluid, a portion of the surrounding fluid is set into motion by the body's pressure field and propagates along with the body. The volume of fluid that drifts with the solid object is proportional to the volume of the object itself. The ratio of drift volume (V_{drift}) to body volume (V_{body}), called the added-mass coefficient (C), depends only on the shape of the body relative to the oncoming flow. In the case of a vertically stratified fluid such as the ocean, the induced fluid drift caused by vertical motion of a solid body will result in a concomitant change in the total potential energy of the fluid, since higher-density fluid is raised above lower-density fluid during upward body motion (and vice versa during downward body motion; see figure 4.1). The resulting increased interface between the fluid masses of different density will be susceptible to further stirring

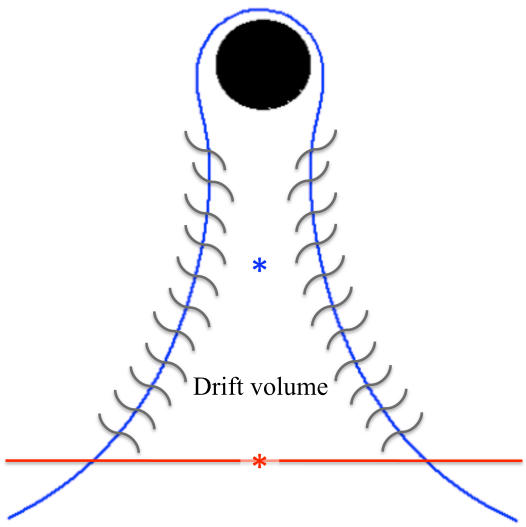

Figure 4.1. Diagram indicating mixing along interfacial region due to the drift mechanism. Red line: initial fluid surface; blue line: deformed fluid surface that encompasses the upward moving body (black circle); gray curved lines: regions of mixing along interfacial regions. Transport of fluid via drift due to a moving body going from less dense to denser fluid results in a displacement of the fluid centroid (red and blue asterisks indicate initial and final positions of the fluid centroid).

by ambient fluid motions and by interaction with neighbouring solid bodies, ultimately leading to molecular mixing [42, 40].

We show that the efficiency of mixing by Darwin's mechanism is dependent on animal shape rather than fluid length scale and unlike turbulent wake mixing, it is enhanced by fluid viscosity [38, 26]. In the limit of Stokes flow, the induced fluid drift becomes infinitely large [41]. Therefore, it provides a means of biogenic mixing that can be equally effective in small zooplankton and large mammals. A theoretical model for the relative contributions of Darwinian mixing and turbulent wake mixing is created and validated by in situ field measurements of jellyfish swimming using a newly developed scuba-based laser velocimetry device [66]. Extrapolation of these results to other animals is straightforward given knowledge of the animal shape and orientation during vertical migration. Based on calculations of a broad range of aquatic animal species, we show that biogenic mixing via Darwin's mechanism can be a significant contributor to ocean mixing and nutrient transport.

4.2 Methods

4.2.1 Defining a Biologically Relevant Mixing Efficiency

In order to establish the importance of biogenic mixing in the oceans, a quantitative metric that compares biogenic mixing with common mixing processes in the physical oceanography literature should be used. To quantify the mixing effects of swimming-induced animal fluid transport, we will calculate the flux Richardson number (R_f; [135]). The flux Richardson number is defined from the turbulent kinetic energy equation [127], and is the ratio between the buoyancy flux and the net mechanical energy to sustain turbulent motions. In other words, the flux Richardson number is a quantity that describes the efficiency of a mixing process [44]. For most mixing processes, the buoyancy flux in the fluid is equivalent to the change in potential energy state (ΔPE) as denser fluid is lifted into less dense fluid and vice versa [79, 9, 104]. The mechanical energy available to generate mixing by an animal is the kinetic energy in the fluid (ΔKE) induced by an animal's swimming motions. Therefore, for swimming animals R_f is defined as

$$R_f = \frac{\Delta PE}{\Delta KE} = 2\frac{m\,g\,\Delta h}{\rho \int\limits_V v^2\,dV}, \tag{4.1}$$

where m is the mass of the fluid being transported, g is the gravitational acceleration and Δh is the displacement of the transported fluid's centroid after the mixing is complete. The kinetic energy is evaluated volumetrically (V) from the velocity field data acquired from digital particle image velocimetry (DPIV) analysis [140, 133, 66]. To determine the change in potential energy, we will utilize planar laser induced fluorescence (PLIF; [71, 31, 45, 25]) measurements in the field.

4.2.2 Experimental Measurements of Mixing Efficiency

In situ measurements of jellyfish swimming (*Mastigias sp.* ranging from 1 to 10 cm body diameter) were conducted in a lake in Palau during September 2008. Video recordings of fluorescein dye injected upstream of individual jellyfish enabled empirical observation of the induced drift effect described in section 4.1. We used a self-contained underwater velocimetry apparatus (SCUVA; [66])

to allow a scuba diver to directly measure the wake kinetic energy of freely swimming jellyfish in the water column. The scuba diver operating the system remained motionless in the water column as animals swam freely into the plane of a 1 mm thick vertical sheet of light produced by a 250 mW, 532 nm diode-pumped solid-state laser. The laser sheet illuminated naturally suspended particulate matter in the marine lake environment (typically 10–100 microns), and the particle motion induced by the swimming animal was recorded at 30 Hz using a high-definition (HD, 1920×1080 pixels) CMOS camera (Sony Corporation). Consecutive images of each video were analyzed with an in-house DPIV algorithm, using an interrogation window size of 64×64 pixels and 50% window overlap. A representative case of jellyfish swimming was selected for in-depth analysis of the wake kinetic energy.

The wake kinetic energy was computed at each node i of the velocity field according to the definition $KE_i = \frac{1}{2}\rho V_i |\vec{u_i}|^2$, where ρ is the ambient water density (1020 kg m^3), V_i is the volume of the node (assuming radial symmetry about the animal body axis), and $|\vec{u_i}|$ is the magnitude of the velocity (i.e., the speed) at each node. The total wake kinetic energy was determined by summing the energy at each of the nodes in the wake. The maximum increase in wake kinetic energy during each swimming cycle, ΔKE, was identified from the temporal trend of the wake kinetic energy measurements. The corresponding dissipation rate ϵ was estimated as $\Delta KE/m\,T_c$ where m is the mass of fluid encountered by the animal per swimming cycle and T_c is the duration of bell contraction.

In addition, PLIF measurements of an artificially created stratified layer in midwater enabled measurement of the change in fluid potential energy caused by a jellyfish swimming through the layer. A sheet of rhodamine fluorescent dye mixture of known density, ρ_{dye} ($< 1\%$ above ambient fluid density, or $\rho_{ambient}$), was injected upstream of swimming *Mastigias sp.* and recorded using the SCUVA optics. Fluorescence intensity was correlated with fluid density via an a priori laboratory calibration. The displacement, Δh, of the dye centroid along the direction of animal swimming (not necessarily vertical) was measured using an in-house image processing code (with post-processing steps shown in figure 4.2), and was used to infer the change in fluid potential energy for a vertically

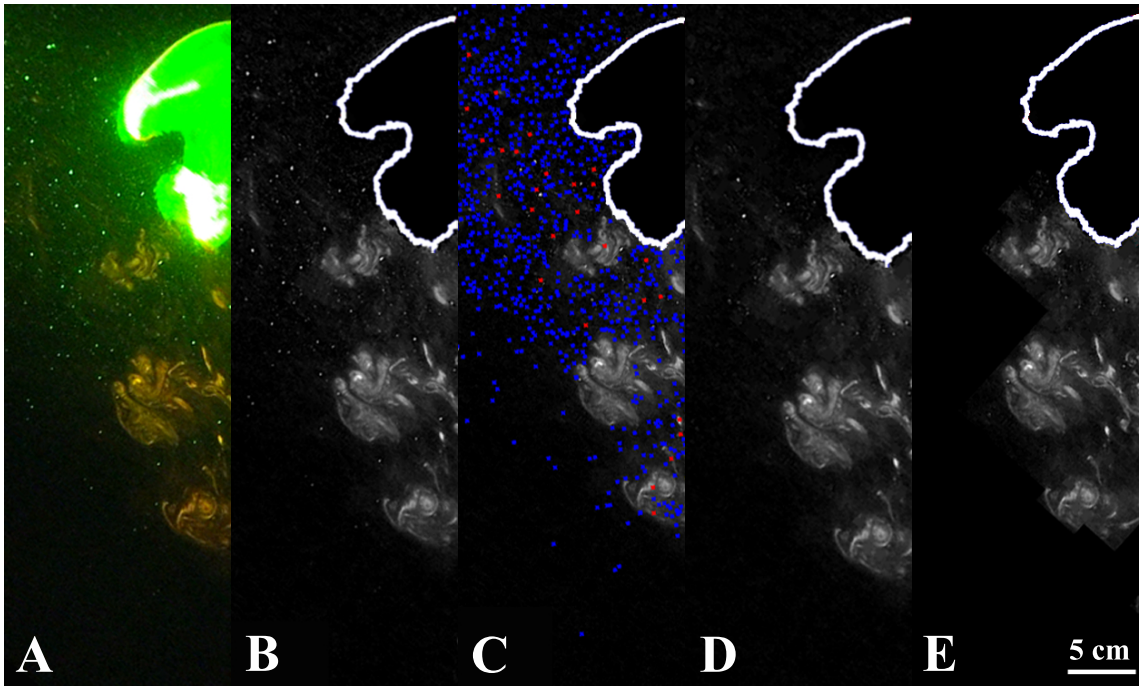

Figure 4.2. Post-processing of PLIF images used for the flux Richardson number measurements. A, The raw color video image of the dye field after *Mastigias sp.* swims through the dye patch. B, Color channels are adjusted to reveal the dye, however bright particles still remain in the image. C, Object analysis reveals the number of separate objects identified in the field of view. Objects with an area less than a predefined threshold are removed and their corresponding image intensity is adjusted to the average value of their neighboring pixels (indicated by blue dots). Objects with an area greater than the threshold are indicated by red dots. D, The smoothed dye field is revealed after averaging is complete. E, The dye field is further defined by selecting objects with areas greater than a second threshold value.

migrating animal as $\Delta PE = (\rho_{dye} - \rho_{ambient})\, V_{dye}\, g \Delta h$, where V_{dye} is the volume of injected dye.

4.2.3 Numerical Simulations of Fluid Transport due to Moving Bodies

The motion of fluid particles induced by the passage of two-dimensional bodies of circular and elliptical cross-section through viscous flow at $Re = 1$, 10, and 100 was computed using the Fluidica software tool [125]. Figure 4.3 shows the theoretical limits for the added-mass coefficient as a function of body shape in two and three dimensions. From figure 4.3, we note that the relationship between body shape and coefficient of added mass (and consequently drift volume) is qualitatively the same for elliptical cross sections (figure 4.3, dashed line) and spheroids (figure 4.3, solid line). Hence, we will investigate the effect of elliptical cross sections (or simulate two-dimensional flows) in

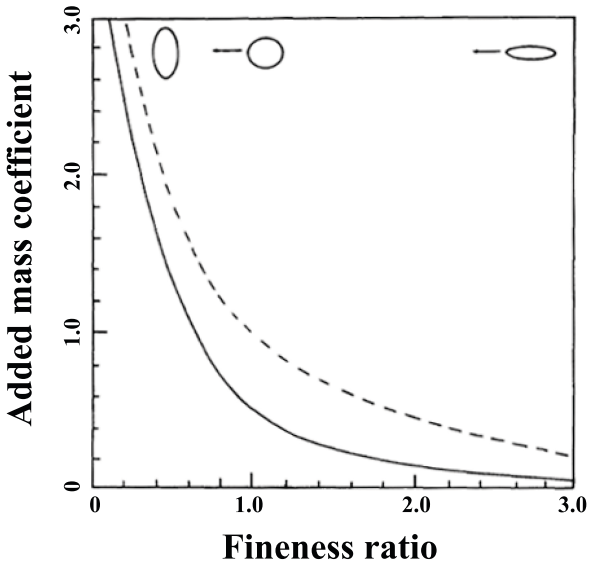

Figure 4.3. Theoretical added-mass coefficients as a function of the length-to-diameter (or fineness) ratio for spheroids (three-dimensional bodies, solid line) and elliptical cylinders (two-dimensional surfaces, dashed line). The fineness ratio is the ratio of the axis parallel to the direction of motion to the axis perpendicular to the direction of motion. Image adapted from Daniel [33].

order to reduce the complexity of the numerical analysis and the inherent computational costs. Our findings in two dimensions will serve as an upper bound to the real, measured flows. Particles in the flow were advected according to the local velocity u, and the drift volume was calculated assuming axisymmetry.

4.3 Results

As *Mastigias sp.* swims through a patch of fluorescein dye originally placed in front of its body, the dye patch is stretched and stirred into the ambient fluid after multiple swimming cycles (figure 4.4B). Aside from illuminating wake structures in the form of vortex rings [30, 27], the dye also reveals a volume of fluid that follows the animal as it continues to swim forward. This phenomenon of fluid transport is known as drift, which was discussed in more detail in section 4.1.

We demonstrate the effect of viscosity by computing the flow around bodies of circular cross-section and diameter D migrating in a viscous fluid at velocity U. The relative effect of viscosity (ν) was manipulated by varying the Reynolds number of the flow, $Re = U\,D/\nu$, from 1 to 100. Since the

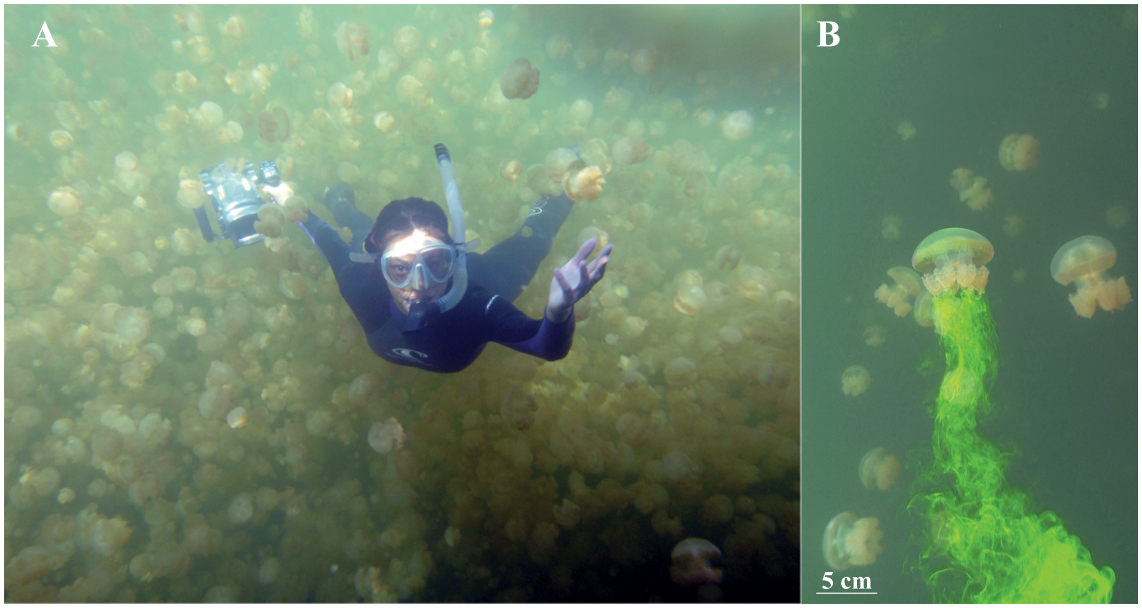

Figure 4.4. Field measurements of induced drift during jellyfish swimming. A, Image of author in water column handling the camera for laser velocimetry. Photo credit: W. M. Graham. B, Induced forward drift of dye behind a swimming *Mastigias sp.* Image is rotated 90 degrees, i.e., gravity acts from left to right in the image.

drift volume increases monotonically with time in the presence of viscosity [41], we calculated a nominal drift after each body migrated the same distance. Figure 4.5A shows substantial enhancement of induced drift at decreasing Reynolds numbers. The drift volume in each case is significantly larger than for an equivalent body in an unbounded, inviscid fluid, for which the added-mass coefficient $C = 1$ [75].

The dependence of Darwin's mechanism on body shape is investigated by computing the fluid drift induced by bodies of elliptical cross section at $Re = 10$. Figure 4.5B shows that drift volume decreases with increasing fineness (i.e., length-to-diameter) ratio, consistent with known trends (see figure 4.3). However, the magnitude of the drift induced by even the most prolate body is substantial due to viscous effects at low Reynolds numbers.

The net mechanical energy required to sustain mixing can be determined by using the velocity fields obtained from the DPIV measurements (figure 4.6). In addition, the location of the dye patch (identified by its centroid) before and after an animal swims through it provides a measure of the buoyancy flux (figure 4.7). Calibrated density fields from the fluorescence intensity of the dye are

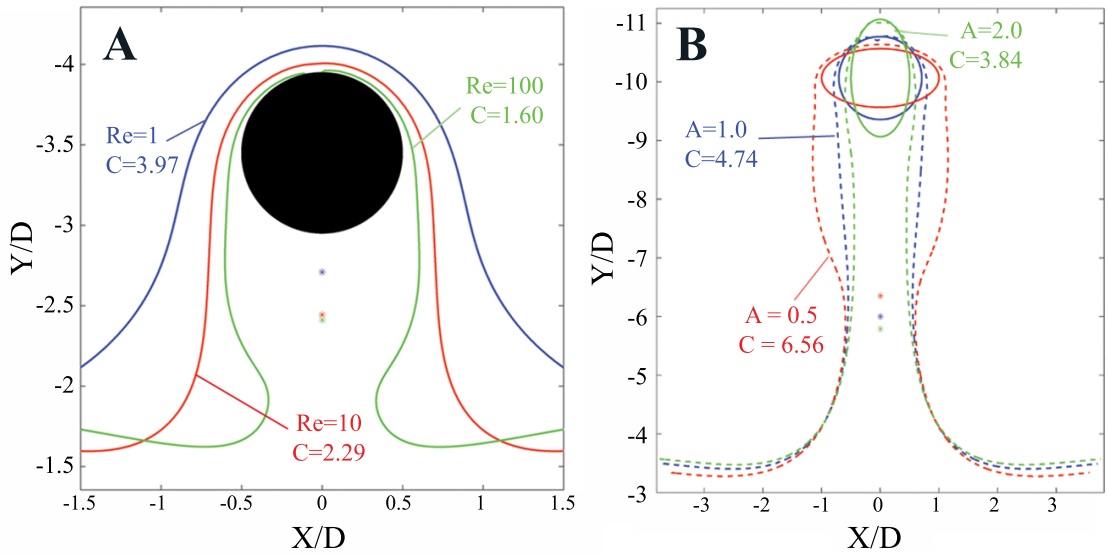

Figure 4.5. Numerical simulations of induced vertical drift of initially horizontal layers in the presence of fluid viscosity. A, Simulation of induced fluid drift due to vertical migration of a circular cross-section at $Re = 1$ (blue), 10 (red), and 100 (green). The cylinder moves vertically at unit velocity in each case. The area of induced drift bounded by each curve at the instant shown in the figure and its initial unperturbed horizontal position is indicated in the figure, normalized by the area of the circle. Induced drift increases with decreasing Re. B, Simulation of induced fluid drift due to vertical migration of elliptical cross sections at $Re = 10$. The fineness (i.e., length-to-diameter) ratio A and the normalized drift area C are indicated for each case. Induced drift increases with decreasing fineness ratio. Note that the values of C differ for the circle in panels A and B due to the difference in time at which the drift area is measured in each case.

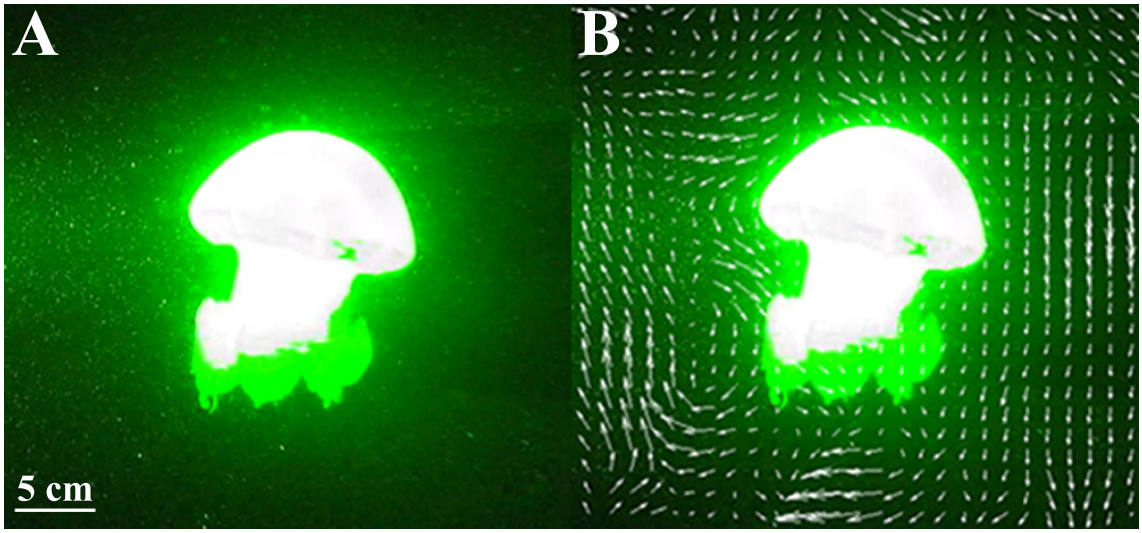

Figure 4.6. A, In situ measurement of *Mastigias sp.* swimming through the laser sheet. B, Corresponding velocity fields at same time instant.

shown in figure 4.8, where the minimum fluid density corresponds to the ambient fluid density (or $\rho_{ambient} = 1018$ kg m^{-3}) and maximum fluid density corresponds to the dye density (or $\rho_{dye} = 1023$ kg m^{-3}). The centroid displacement, Δh is computed from the vertical change in location of the dye centroid (figure 4.8A and B, white dot). From the DPIV and PLIF measurements (where ΔKE and ΔPE are quantified, respectively) the flux Richardson number can be experimentally determined.

The flux Richardson number is given by the ratio $\Delta PE/\Delta KE$ and is 24±18% for a representative measurement, with the primary source of measurement uncertainty being the value of V_{dye} estimated from the dye images. Table 4.1 summarizes the flux Richardson number for reported physical mixing processes and the jellyfish result for biogenic mixing. The corresponding Brunt-Vaisala buoyancy frequency (N) is computed according to the definition $N = \sqrt{-\frac{g}{\rho_0}\frac{d\rho}{dz}}$, where dz is estimated based on the length scale of the dye patch before interaction with the animal ($dz \approx 2$ cm). The corresponding Ozmidov buoyancy length scale is found according to the definition $B = \sqrt{\epsilon/N^3}$ and is nominally 4 cm. Since the Ozmidov length scale of the injected dye layer ($B \approx 4$ cm) is significantly smaller than the natural buoyancy length scale of the lake [55], the observed dynamics are decoupled from ambient fluid motions. Additionally, the buoyancy length scale of the dye is approximately two

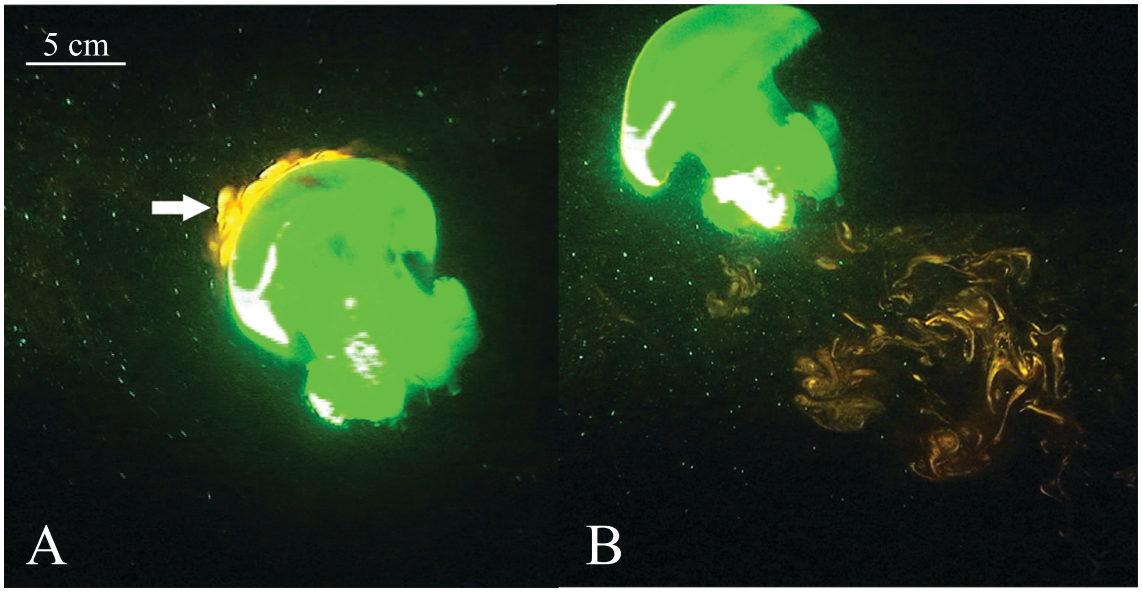

Figure 4.7. A, In situ measurement of *Mastigias sp.* swimming through an artificially created density stratification (indicated by white arrow). Red fluorescence intensity is proportional to fluid density. B, Mixed density field following passage of *Mastigias sp.* The centroid of the density field is shifted in the direction of animal swimming (see figure 4.8). For a vertically migrating animal, this will result in a change in the potential energy of the fluid.

orders of magnitude larger than the mean ocean (based on the background dissipation rate and the range of mean buoyancy frequencies in the ocean [74, 128]), indicating that our measurements show biogenic mixing in strongly stratified conditions.

Table 4.1. Summary of reported flux Richardson numbers of physical ocean mixing processes compared to biogenic mixing by an individual *Mastigias sp.*

Mixing Process	R_f	Reference
Grid-generated turbulence	0.06	[104]
Vortex rings	0.15	[79]
Jellyfish swimming	0.24	[67]
Kelvin-Helmholtz instability	0.25	[120]
Rayleigh-Taylor instability	0.35	[80]
KH-Holmboe wave interactions	0.45	[92]

Since the shape of the induced drift region is approximately conical during the first few body lengths of travel through the stratified layer [38], the contribution of induced drift to the measured fluid displacement Δh was estimated based on the distance from the base to the centroid of a right circular cone (with base and slant height equal to the characteristic length, L, of the animal). Hence,

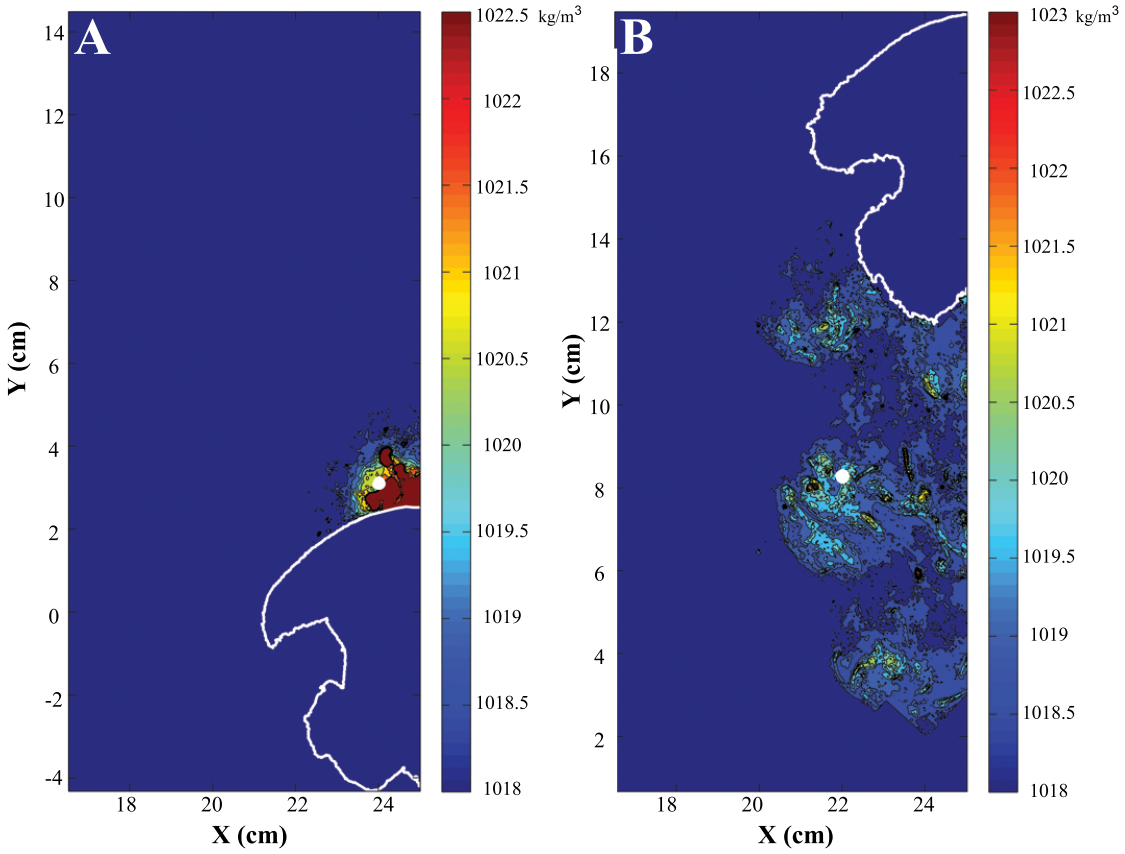

Figure 4.8. Resultant density field from planar laser-induced fluorescence measurements. A, Calibrated density field prior to passage of *Mastigias sp.* through density stratification. B, Calibrated density field following passage of *Mastigias sp.* through density stratification. Change in dye mass centroid is indicated by shift in white dot from panel A to panel B. Animal position is indicated by white outlines. Images are rotated to vertical orientation.

the contribution from induced drift to the measured change in dye centroid, Δh_{drift}, was estimated as $\sqrt{3/64}\,L$. For the *Mastigias* measurement, $\Delta h_{drift}/\Delta h \approx 0.9$, indicating a dominant contribution of induced drift to the change in fluid potential energy. The measurements demonstrate that the mixing process was dominated by the induced drift effect, with 90% of the potential energy increase attributable to drift. Therefore, neglect of the contribution of drift in theoretical models of the mixing efficiency (i.e., flux Richardson number) will result in an order-of-magnitude underestimate.

4.4 Discussion

The contribution of induced fluid drift relative to turbulent wake mixing can be predicted by considering the swimming efficiency of the animal. The Froude propulsive efficiency, the ratio of usable energy for overcoming drag to the total fluid energy input during locomotion, can be written as

$$\eta_F = \frac{F_D\,U}{F_D\,U + \epsilon}, \tag{4.2}$$

where F_D is the drag force on the animal, U is the swimming speed, and ϵ is the flow of kinetic energy into the wake per unit time. As an order-of-magnitude estimate, the drag per unit fluid density can be approximated as $F_D \approx V_{drift}^{2/3}\,U^2$, where for the sake of convenience, the characteristic area over which hydrodynamic forces act is derived from the drift volume (i.e., $V_{drift}^{2/3}$). The wake energy flux per unit time ϵ can be partitioned into the portion that contributes to changes in the potential energy of the fluid ($K\,N^2$), and the portion that is dissipated as heat by the fluid viscosity (i.e., $(1-\Gamma_\epsilon)\,\epsilon$), which depends on the mixing efficiency Γ_ϵ. For animals smaller than the characteristic buoyancy length scale of the stratified fluid, the mixing efficiency can be estimated as $\Gamma_\epsilon \approx \left[\frac{V_{drift}^{1/3}}{(\epsilon/N^3)^{1/2}}\right]^{4/3}$, where the characteristic length scale of the body is again derived from its drift volume (i.e., $V_{drift}^{1/3}$). Substituting these expressions into equation (4.2), we arrive at the following relationship,

$$\eta_F = \frac{V_{drift}^{2/3}\,U^3}{V_{drift}^{2/3}\,U^3 + K\,N^2\,V_{wake} + \left[1 - \frac{V_{drift}^{4/9}}{(\epsilon/N^3)^{2/3}}\right]\epsilon\,V_{wake}}, \tag{4.3}$$

where we have formulated the swimming efficiency in terms of properties of the animal (i.e., its swimming speed U and kinetic energy flux per unit time ϵ into the turbulent wake of volume V_{wake}), the drift volume (V_{drift}), and the ocean (i.e., turbulent diffusivity K and Brunt-Vaisala buoyancy frequency $N = \sqrt{-\frac{g}{\rho}\frac{d\rho}{dz}}$). The latter two terms in the denominator of equation (4.3) together represent the kinetic energy flux per unit time (ϵ) lost to the turbulent wake as the animal swims; the existing debate over biogenic mixing has focused on their relative magnitudes [74, 135]. However, the present simulations and experiments demonstrate that this is only one, potentially small, component of biogenic mixing. Using equation (4.3) and knowledge of the swimming efficiency, we were able to draw conclusions regarding both the relative contributions of induced drift and turbulent wake mixing in animal swimming, as well as the absolute magnitude of the effect of the Darwinian mechanism on ocean mixing.

Qualitatively speaking, a higher swimming efficiency leads to a larger relative contribution of induced fluid drift to mixing compared with turbulent wake energy. Indeed, in the limit of perfect swimming efficiency, no energy is lost to the wake and Darwin's mechanism is the only one available for fluid mixing. Swimming efficiencies as high as 90 percent are reported in the literature on aquatic animals [46], consistent with our experimental observations that Darwin's mechanism can dominate over turbulent wake mixing. Even in the limit of low swimming efficiency, Darwin's mechanism will still contribute to mixing since induced drift will persist as long as the animal is moving.

For small animals, i.e., those with length scale smaller than the Ozmidov scale B, turbulent mixing becomes inefficient due to the effects of fluid viscosity [135]. In these cases, Darwin's mechanism will be the dominant source of mixing irrespective of the swimming efficiency.

To determine the absolute contribution of Darwin's mechanism to ocean mixing, we note that previous studies of animal wake turbulence estimate kinetic energy production rates on the order of 10^{-5} to 10^{-4} W kg^{-1} for animals spanning a range from 10^{-3} to 10^{1} m in length and 10^{-5} to 10^{3} kg in mass [59]. Since the swimming efficiency is of the order 10^{-1} to 1 across the same range of animals [59], we conclude based on equation (4.3) that the mixing power provided by induced fluid drift is at least of the order 10^{-5} to 10^{-4} W kg^{-1}. This is comparable with the turbulent dissipation

observed due to physical processes (e.g., winds, tides, etc.; [74, 135, 59, 35]). By a similar argument, the estimated 10^{12} watts of total turbulent kinetic energy input per unit time by marine animals [35] indicates that the global contribution to mixing by Darwin's mechanism is also in the range of 10^{12} watts. This, too, is of the same order of magnitude as the global contributions of winds and tides. The local contributions of swimming animals to ocean mixing will depend on details of the migration behavior, which can be heterogeneous even within a single school [93].

We consider these estimates to be conservative in an unstratified fluid since they are based on the fluid transport induced by individual animals swimming in isolation. However, in the case of a stratified fluid, we would expect fluid transport to be limited to specific length and time scales, potentially reducing the global contribution of biogenic mixing. Chapter 5 attempts to address fluid transport in a stratified fluid and modifies the biogenic mixing contribution to the global ocean mixing energy budget. The drift volumes of neighboring animals in an aggregation may interact via their boundary layers to further enhance vertical transport, thereby increasing the horizontal scale of the vertically drifting fluid mass to the horizontal extent of the entire aggregation of animals. However, studies of fluid transport by a single animal cannot be simply superimposed to extrapolate the effect of an entire school of migrating swimmers. Extensive theoretical and experimental analysis is required to understand whole-population dynamics (mentioned briefly in chapter 6). Further, we have not included in our estimates the effect of passively sinking particulates (e.g., marine snow, fecal pellets, etc.) that induce a drift of the surrounding fluid with potential implications for downward transport to the deep ocean (e.g., carbon sequestration).

A common criticism for biogenic mixing via drift is related to reversibility of fluid transport as animals migrate upwards and downwards daily. If a small animal ($Re \ll 1$) transports fluid via drift during its diurnal migration, one might argue that the net transport of fluid is nearly zero since the animal returns to its initial position. This statement would be true (assuming animal swimming behavior and characteristics are repeated exactly throughout migration) if we ignore all other physical mixing processes in the ocean that may be active. Diffusion will occur as long as gradients in a scalar field are present. Stirring of fluid by migrating animals via drift would create

gradients in the temperature or salinity fields, thereby providing conditions for diffusion. If we define a diffusive time scale (see chapter 5 for details) based on the thermal diffusivity of seawater and characteristic length scale of a swimmer, we find that the diffusive time scale is on the order of 10^4 s; this is less than the average time associated with a diurnal migration ($\sim$ 8 hrs). Therefore, by diffusion alone, the fluid transported by swimming animals via drift will irreversibly diffuse and mix with its surroundings before the end of migration.

Finally, we note that simulating swimming animals as passive bodies that move by an applied external force is an oversimplification. Therefore, in this work we are careful to provide additional support before making conclusions about the global impact of animal swimming on the ocean. In the other extreme, animals are often computationally modeled as a point-force dipole, commonly referred to as the self-propelled swimmer model [16, 8]. In the limit of steady motion, the self-propelled swimmer generates no net force on the fluid since the contributions of time-averaged thrust and drag on the body offset [126]. Therefore, the behavior of the flow field surrounding a moving body or self-propelled swimmer are drastically different, providing limits of animal-induced drift. To be sure, animal swimming is an unsteady process and cannot be accurately modeled as a force dipole. In the context of this work, the simulations of passive particles are meant to illustrate the drift effect only. From the field observations of animal-induced drift (figure 4.4), the derivation of equation (4.3), and the estimates of global turbulent kinetic energy dissipation by animals from Dewar et al. [35], the case for biogenic mixing via drift is compelling.